HYDRO-IONIC MICROTHRUSTER FOR LOCOMOTION IN LOW-REYNOLD'S NUMBER IONIC FLUIDS

Daniel L. Magley[1], Vinayak Narasimhan[2], and Hyuck Choo[1,2]
[1]Department of Electrical Engineering, California Institute of Technology, Pasadena, CA, USA
[2]Department of Medical Engineering, California Institute of Technology, Pasadena, CA, USA

ABSTRACT

We have demonstrated a fast, extremely power-efficient, hydro-ionic microthruster that utilizes electro-osmotic propulsion for operation in a low Reynolds-number ionic environment. Powered by an onboard power supply, the microthruster achieves speeds of up to 5.24 cm/s (131 body-lengths/s) while consuming less than 252 nW/(Bodylength/s). It is 31% faster and ~10^3 times more energy-efficient than prior designs. Including the onboard Al-air battery consisting of an Al anode and an Au cathode, the microthruster measures 1400µm (H) × 1400µm (W) × 400µm (L) in dimension and contains a 1000µm-wide, 300µm-long cylindrical thruster channel in the center. With significantly improved speed and drastically higher energy-efficiency, the microthruster opens up new possibilities for various self-powered biomedical applications that can operate within the power budget of modern implantable and integrable microscale batteries and bio-fuel cells.

INTRODUCTION

Efficient propulsion for locomotive implants in low Reynolds-number environments holds many potential medical applications including minimally-invasive surgery, diagnostics, targeted drug delivery, microfluidic pumps, and *in-vivo* gene therapies, which could be made possible through utilization of the human circulatory system. Previous efforts in developing low Reynolds propulsion methods can be divided up into two categories: relying on viscous forces such as viscous tension for helical tails; and utilizing momentum transfer to generate their thrust such as with bubble jet propulsion [1] (Fig.7).

Momentum-transfer-based methods can achieve high speeds, but due to low Reynolds number suffer great drawbacks in terms of efficiency due to viscous forces dominating over momentum forces in the fluid medium. As an example, prior methods utilized momentum transfer as their propulsion mechanism to achieve relative speeds of up to 100 body-lengths/second (BL/s), but could only maintain movement for 0.360 seconds due to their low energy efficiency [1].

Viscosity-based methods, specifically those that utilized an artificial helical flagella design, were able to achieve 20-30 BL/s using either magnetic pulling or electro-osmosis as a means to spin the tail and generate viscous tensions [1-2]. The most efficient approach, in terms of the (BL/s)/watt ratio, was demonstrated by a device using magneto-hydrodynamic propulsion, in which the device was made to oscillate like a fish's tail generating viscous tensions. The device achieved 1 BL/s (0.53 cm/s) speeds while consuming 250 µW [3]. Current implantable bio-fuel cells can provide about 218 µW/10mm^2, potentially occupying a large space to provide the 250 µW power requirement for the current most efficient method and leaving no power for additional functionality [4]. A more efficient and faster propulsion method is necessary for self-powered locomotive implants.

DESIGN/OPTIMIZATION

To realize a faster more efficient propulsion method, we aimed at creating a hybrid method, one which focused on generating its efficiency from viscous forces while relying on momentum transfer to generate the actual thrust of the device. We recognized electro-osmosis as a physical phenomenon where the viscosity of the fluid was directly proportional to the momentum transfer from the fluid at the Debye length to the fluid above it. This means that the efficiency of using electro-osmosis for generating a velocity profile that will result in momentum transfer is proportional to the viscous forces in the fluid. Therefore, we can directly use the momentum transfer of bulk fluid flow induced by electro-osmosis as the propulsion force for a device to realize our hybrid method.

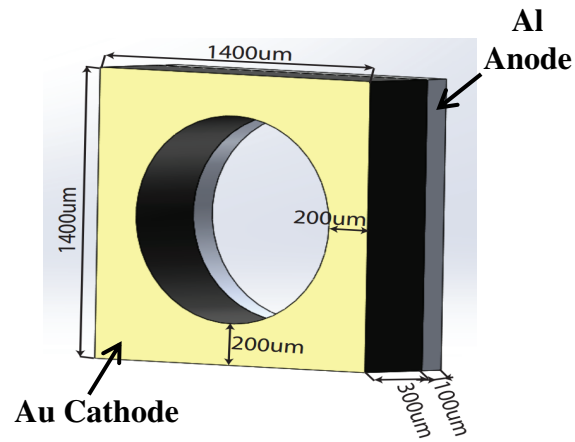

Figure 1: Schematic of the Microthruster with an onboard redox Al-air Battery.

A cylindrical channel was chosen in order to optimize the effect of the boundary condition imposed by electro-osmosis. Using the COMSOL Microfluidics module, we optimized the dimensions of the cylindrical channel with electrodes on the opposite sides (Fig.1). We simulated (1) the resulting velocity profiles of the device when 250mV was applied to each electrode (Fig.2(a)); and (2) the drag forces (F_D) experienced by the device when traveling at 1cm/s speeds (Fig.2(b)) for pipe diameters ranging from 250-1750 µm at every 250 µm. We then calculated the net propulsion force (F_{net}) of the device for each diameter using equation 1.)

$$F_{net} = \rho_{fluid} A_{channel} \left(V_{fluid} - V_{Device}\right)^2 - F_D \qquad (1)$$

where ρ_{fluid}, $A_{channel}$, V_{fluid}, and V_{device} are the fluid's density, the cross-sectional area of the channel, and the

velocities of the fluid and device, respectively (Fig.2(c)). We found an optimal diameter ranged between 1000–1500 µm for 300µm long channels.

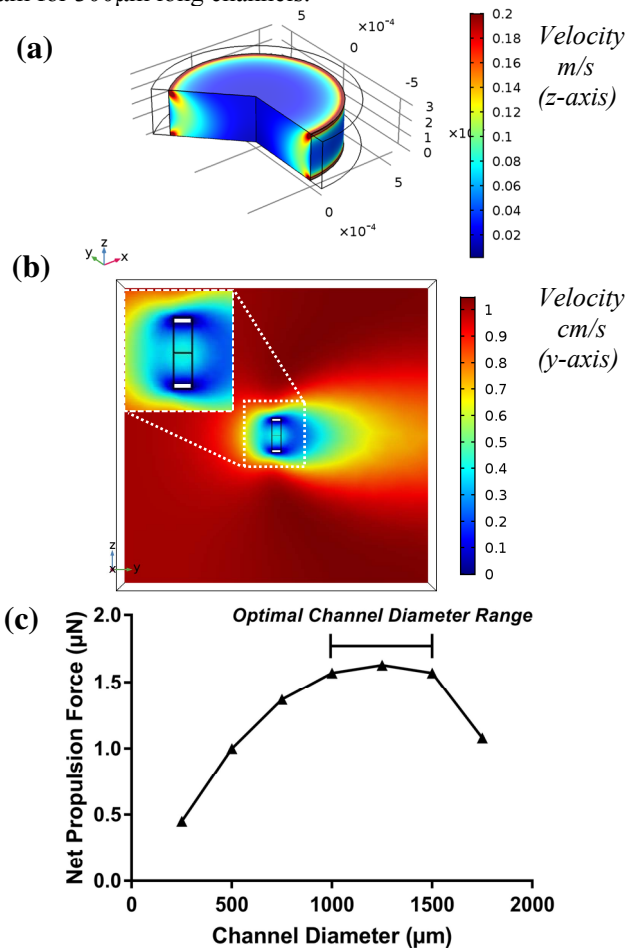

Figure 2: Design Optimization: (a) COMSOL simulation of the fluid velocity profile inside the cylindrical channel at 250 mV; (b) COMSOL simulation of the fluid drag profile surrounding the microthruster subject to 1cm/s movement speed (side view); and (c) the calculated net propulsion force obtained using the simulation results and Eq. (1). The optimal channel diameters ranged between 1000-1500 µm.

FABRICATION

The device was fabricated using a single mask process. On a 300µm-thick p-doped silicon wafer, we electron-beam-evaporated 300nm-thick Al_2O_3 hard mask and patterned using lift-off. Subsequently, we used a Bosch-DRIE process to punch through the substrate, releasing the devices. Finally, we electron-beam-evaporated 200nm-thick Au on one side of the structure. The Al-air battery was completed by assembling a 100µm-thick Al foil on the other side. For the mobility experiment, a thin layer of hydrophobic polymer was coated on the 300µm-long top Si face to keep the device upright in solution.

DEVICE CHARACTERIZATION

All experiments were carried out using devices with a 1000µm-diameter channel in 7680 µS/cm saline solution to approximate the median of blood's conductivity ranging from 2000-15000 µS/cm that would depend on blood cell concentrations [5].

Battery Voltage Characterization

A device with an Al-air battery was submerged in saline solution, and the voltage between the Al and Au electrodes was collected at 100 Hz for 120s (Fig.3). A steady state operating voltage of approximately 250mV was observed.

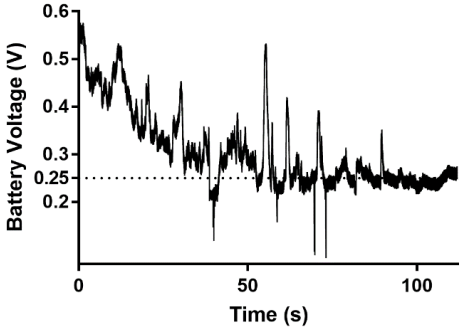

Figure 3: Recorded output voltages of the onboard Al-air battery on a 1000µm channel device in saline solution.

Device Power Consumption

We actuated a submerged double sided Au-Au device by applying 250mV and caused the fluid to flow. A current of 14.7µA was measured flowing through the device indicating an average power usage of 3.68µW. The resistance of the device was measured before and after submerging as shown in Table 1.

Table 1: The resistances measured across the device pre- and post-submersion. The pre-submersion resistance can be interpreted as the resistance of the entire device and was purposefully engineered high to minimize resistive heating losses. The resistance of the submerged device can be assumed to originate solely from the fluid's resistance in the device channel.

State	Interpretation	R_{Value}
Pre-Submerging	R_{Device}	55 MΩ
Post-Submerging	R_{Fluid}	53.2 kΩ

Flow Rate

A double-sided Au device was embedded in the center of a 1200µm (H) × 1200µm (W) × 1800µm (L) rectangular channel (Fig. 4), which connected the two separate 10cm (W) × 5cm (L) × 5mm (H) rectangular reservoirs at the bottom of the separating wall. 250 mV was applied across the imbedded device and 200 µL of Propylene Glycol FD&C Blue 1 dye was deposited on the one side of the channel, which we defined as an upstream of expected fluid flow (Fig. 4(a)). The time it took for the dye, once it had entered the connecting channel, to exit into the opposing reservoir was determined to be 5.21s via video-frame analysis taken at 24 frames per second (fps). The control with no voltage applied to the device took over 600s after entering the channel to exit into the other side. This indicated that osmotic dispersion of the dye had negligible contribution to the dye's movement through the channel (Fig. 4(b)). Dividing the volume of fluid contained inside the center channel by the time the dye took to travel through it, we obtained a flow rate of 0.460 µL/s and an average fluid velocity of 0.586 cm/s through the 300µm-long channel.

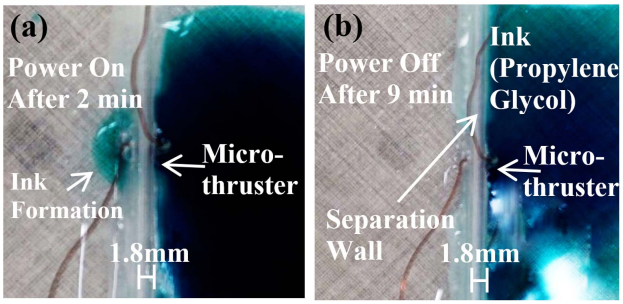

Figure 4: Flow-rate test for a double-sided Au device separating two 25ml reservoirs of saline solution. The two reservoirs are separated by a 1.8mm thick wall embedded with a microthruster. 200 µL of Propylene Glycol FD&C Blue 1 was deposited in the right reservoir to see the propulsion through the cylindrical ionic thrust channel. (a) microthruster power on: after only 2 min, a noticeable ink formation is observed in the left reservoir; and (b) microthruster power off: no movement of ink even after 9 min.

Mobility Experiment

A Type 304, 10" diameter Stainless Steel bowl was grounded and filled with 0.4 L of NaCl solution (7680 µS/cm). We chose a type 304 stainless steel bowl due to its low half-cell potential (-0.08 V) and ability to be grounded [6]. A camera was positioned over the bowl and set to record the entire bowl at 4k resolution and 24 fps. A control device, identically fabricated except with no Al attached to it, had solution pipetted into its center channel to avoid air bubbles and was floated in the bowl, but it showed no movement as expected.

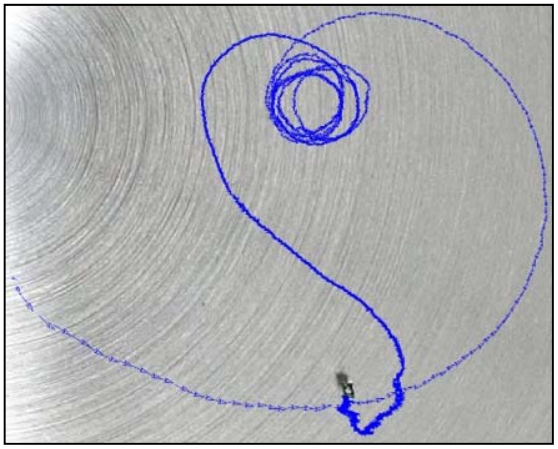

Figure 5: The vectored path of the device movement powered by the onboard battery in saline solution and tracked using a 4K-24fps camera.

The active device also had solution pipetted into its center channel to avoid air bubbles. After 30 seconds the device was placed in the center of the bowl with the hydrophobic polymer side facing upwards towards the camera. Upon placing in solution, the device immediately started moving in a large circular motion and then moved in several smaller circles before taking on one final large circular sweep forming a sort of heart shape (Fig.5). The control showed no detectable movement during the entire recording period.

Analysis

Confirming Electro-Osmotic Propulsion

The mobility experiment video was uploaded and analyzed using video physics analysis software. The center of mass of the device was marked frame by frame from the point of release to the end of motion. The video scale was calibrated using the diameter of the bowl, which was 25.4 cm, and the time between two successive frames was obtained from the timestamp on each frame. The distance that the device covered between two successive frames was divided by the time between the frames to obtain the device's velocity. Fig.6 shows a graph of the device's velocity throughout the video. Note from the inset that there was initially a period of acceleration up to 5.24 cm/s, followed by an exponential decay in velocity to a steady state around 1 cm/s in the first 10s and then by a gradual decay over the next 52 seconds to a halt. The average velocity for the entire period was 0.583 cm/s.

This behavior is expected from the initial drop in voltage seen in Fig.3. The voltage of the battery dropped as a layer of oxide formed over the Al anode and limited the reaction rate. This caused the steady state velocity of V_{fluid} from electro-osmosis to drop and thus the net propulsion force described by Eq. 1; and allowed for a period of rapid deceleration during the voltage drop followed by a slow deceleration of the device to a halt.

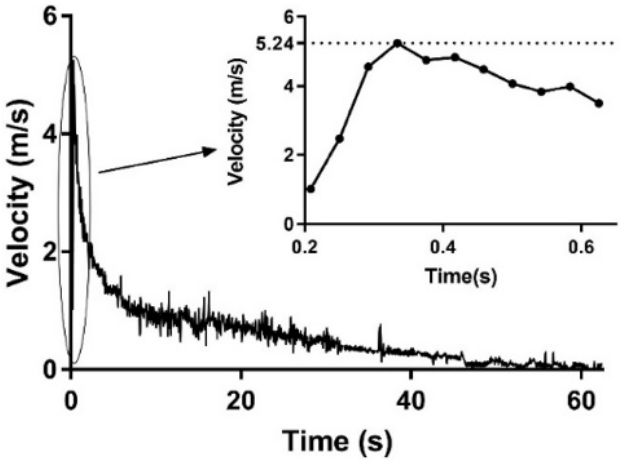

Figure 6: The velocity of the microthruster calculated from a frame-by-frame position analysis. The inset: the first 11 data points showing the micro thruster's acceleration period.

It is also worth noting that the average velocity of the device (0.583 cm/s) shows a very high correlation with the measured average fluid velocity from the flow rate experiment (0.586 cm/s) performed at 250 mV. Considering the agreement between the velocity curve and the expected pattern from the voltage data and also between the flow rate and the velocity data, we can conclude that the propulsion force of the device indeed originated from electro-osmosis.

Device Power Analysis

Using the measured current and resistances from the power consumption experiment, we can derive the resistive heating losses that occur both in the device's Si body and

to the ionic fluid media (Table 2). Note that the total power consumption was calculated from the voltage and current supplied by a power supply, and thus it is the maximum power that can possibly be consumed by the device. When the power is supplied by the battery, its redox reaction can become stressed, and this would lower the output power of the battery, causing the device to operate with power less than 3.68 µW.

Table 2: Power analysis of the device in operation.

Max Total Power Consumed	Power Loss to R_{Device}	Power Loss to R_{Fluid}	Max Power Consumed by Electro-Osmosis
3.68µW	1.14nW	1.17µW	2.51µW

Device-Performance Comparisons

Here we characterized three major aspects of our device so we could compare them with those of prior work (Fig. 7). Because devices can vary in size, we characterized using the body length (BL) of each device as the unit of length. Using the first term in Eq. (1) and knowing the average fluid velocity in the channel from the flow rate experiment, we can calculate the average propulsion force of the device to be 27.0 nN.

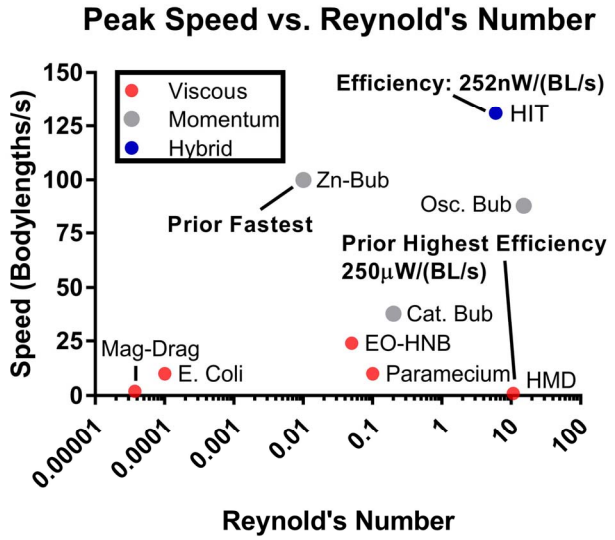

Figure 7: A comparison of our method the Hydro-Ionic Microthruster (HIT) to other notable prior methods and both Prokaryotes and Eukaryotes. Note that our top speed is greater than the prior record of 100 BL/s with 131 BL/s and displays ~10^3 increase in efficiency of W/(BL/s) over prior methods. The cited methods in order of increasing Reynolds Number are [7-8], [1], [2], [8-9], [3], [10].

Using the average device velocity of 0.583 cm/s and maximum power consumption of 3.68 µW of our device, we calculated an efficiency in terms of power consumed per BL/s and obtained 252 nW/(BL/s), nearly a 10^3 increase in efficiency from prior methods [3]. In addition, our device's top speed of 5.24 cm/s translates to a relative speed of 131 BL/s, beating out the prior record speed of 100 BL/s [1].

Conclusion

We have developed an electro-osmotic thruster capable of producing speeds of up to 131 BL/s while operating for 60 seconds, which was both 31% faster and 340 times longer than the prior records, respectively [1]. The device consumes, on average, a maximum power of 252 nW/(BL/s), which is roughly 10^3 times more energy-efficient than the prior record of 250 µW/(BL/s). Overall the faster speed and magnitudes higher efficiency make this propulsion method the first to be both suitable and practical for self-powered, multi-functional mobile operations in micro-scale ionic fluids within the power budgets of available microscale power sources such as implantable biofuel cells. Such capabilities enable new and exciting biomedical applications.

ACKNOWLEDGEMENTS

We would like to thank the Kirk and Marjory Dawson SURF Endowment, Heritage Medical Research Institute, and the Powell Foundation for their funding support.

REFERENCES

[1] Gao, W.; Uygun, A.; Wang, J. "Hydrogen-bubble-propelled zinc-based microrockets in strongly acidic media" *J. Am. Chem. Soc.*, 134, p. 897–900. 2012

[2] G. Hwang et al., "Electro-osmotic propulsion of helical nanobelt swimmers.", *The International Journal of Robotics Research*, 30.7, pp. 806-819, 2011.

[3] D. Pivonka et al., "A mm-sized wireless powered and remotely controlled locomotive implant", *IEEE Trans. Biomed. Circuits and Systems*, 6, pp. 523-532, 2012.

[4] S. Cosnier et al., "Recent advances on enzymatic glucose/oxygen and hydrogen/oxygen biofuel cells: Achievements and limitations", *Journal of Power Sources*, 325, pp. 252-263, 2016.

[5] K. Visser, "Electric conductivity of stationary and flowing human blood at low frequencies," *Engin. in Med. and Bio. Soc., 1989. Images of the Twenty-First Century., Proc. of the Ann. Inter. Conf. of the IEEE Engin.*, 5, pp. 1540 –1542, 1989.

[6] ASM Handbook, Vol. 13, Corrosion of Titanium and Titanium Alloys, p. 675

[7] Tierno, P.; Golestanian, R.; Pagonabarraga, I.; Sagués, F. "Magnetically actuated colloidal microswimmers" *J. Phys. Chem. B*, 112, pp. 16525–16528. 2008

[8] Lauga, E.; Powers, T.R. "The hydrodynamics of swimming microorganisms" *Rep. Prog. Phys.* 2009, 72, 096601; doi:10.1088/0034-4885/72/9/096601.

[9] Solovev, A.A.; Mei, Y.; Ureña, E.B.; Huang, G.; Schmidt, O.G. "Catalytic microtubular jet engines self-propelled by accumulated gas bubbles." *Small*, 5, 1688–1692, 2009.

[10] Feng, J.; Cho, S.K. "Micro Propulsion in Liquid by Oscillating Bubbles." In Proceedings of the 2013 IEEE 26th International Conference on Micro Electro Mechanical Systems, Taipei, Taiwan, 20–24 January 2013; pp. 63–66.

CONTACT

*D.L. Magley, tel: +1-828-5457796; dmag@caltech.edu